

Metrics for Optimizing Searches for Tidally Decaying Exoplanets

BRIAN JACKSON ¹, ELISABETH R. ADAMS ², AND JEFFREY P. MORGENTHALER ²

¹*Department of Physics, Boise State University
1910 University Drive,
Boise ID 83725-1570 USA*

²*Planetary Science Institute
1700 E. Ft. Lowell, Suite 106,
Tucson, AZ 85719, USA*

(Revised 2023 Jul 23; Accepted 2023 Aug 7)

ABSTRACT

Tidal interactions between short-period exoplanets and their host stars drive orbital decay and have likely led to engulfment of planets by their stars. Precise transit timing surveys, with baselines now spanning decades for some planets, are directly detecting orbital decay for a handful of planets, with corroboration for planetary engulfment coming from independent lines of evidence. More than that, recent observations have perhaps even caught the moment of engulfment for one unfortunate planet. These portentous signs bolster prospects for ongoing surveys, but optimizing such a survey requires considering the astrophysical parameters that give rise to robust timing constraints and large tidal decay rates, as well as how best to schedule observations conducted over many years. The large number of possible targets means it is not feasible to continually observe all planets that might exhibit detectable tidal decay. In this study, we explore astrophysical and observational properties for a short-period exoplanet system that can maximize the likelihood for observing tidally driven transit-timing variations. We consider several fiducial observational strategies and real exoplanet systems reported to exhibit decay. We show that moderately frequent (a few transits per year) observations may suffice to detect tidal decay within just a few years. Tidally driven timing variations take time to grow to detectable levels, and so we estimate how long that growth takes as a function of timing uncertainties and tidal decay rate and provide thresholds for deciding that tidal decay has been detected.

Keywords: Exoplanet dynamics (490), Exoplanet tides (497), Star-planet interactions (2177), Transit timing variation method (1710)

1. INTRODUCTION

From the discovery of the first exoplanet orbiting a Sun-like star (Mayor & Queloz 1995), orbital decay powered by tidal interactions has been a point of concern (Rasio et al. 1996). So close to their host stars, short-period gas giants raise substantial tidal bulges on their host stars, large enough that in some cases the bulge has been detected (Barros et al. 2022). For host stars rotating more slowly than their short-period planetary companions revolve, the interaction between this tidal bulge and the planet transfers angular momentum from the orbit to the star, reducing the orbital distance and orbital period (Jackson et al. 2008). The rate at which tidal energy is dissipated within the host star determines the orbital decay rate but, for stars on the giant branch, may be comparable to the stellar luminosity (MacLeod et al. 2018). The stellar dissipation processes, usually quantified via the tidal dissipation parameter Q_* , are likely complex and remain poorly understood (Ogilvie 2014), translating into orders of magnitude uncertainty in Q_* .

Once a gas giant spirals into its Roche limit, a distance determined in part by the stellar and planetary densities (Rappaport et al. 2013), tidal disruption can occur. This disruption may proceed on a timescale set by the tidal decay rate (Valsecchi et al. 2015; Jackson et al. 2016), or the disruption may become unstable and proceed rapidly (Gu et al. 2003; Jia & Spruit 2017). Or, in a more dramatic case, the planet's Roche limit may lie within the star, in which case the tidally decaying planet can be directly accreted by the star (Metzger et al. 2012).

A variety of indirect observational evidence supports these theoretical expectations that short-period planets are disrupted and/or accreted by their host stars: some stars show signs of tidal- or accretion-induced spin-up (Qureshi et al. 2018); main-sequence stars that currently host hot Jupiters tend to be younger on average than main-sequence stars that host planets less susceptible to tidal decay (Hamer & Schlaufman 2019); and some red giant stars exhibit anomalous chemical signatures that may be caused by planetary engulfment (Aguilera-Gómez et al. 2016), and such signatures may also be present but short-lived for main sequence stars (Behmard et al. 2023). De et al. (2023) provided the first direct detection of ongoing planetary engulfment. Based on a large-scale survey, that study reported detection of a low-luminosity optical transient lasting several days, accompanied by a months'-long infrared brightening. These signatures are consistent with engulfment of a planet between 0.1 and 10 Jupiter masses by a Sun-like star about 4 kpc from Earth.

Based on their survey detection statistics and other considerations, De et al. (2023) estimated such events occur at a rate between 0.1 and 1 yr^{-1} . As discussed in Metzger et al. (2012), the engulfment rate scales with Q_* : a value $Q_* \sim 10^6$ translates into about one tidally-driven planetary accretion events per year within the Milky Way. However, the large uncertainties on Q_* mean the actual event rate is likewise highly uncertain. Moreover, Q_* likely depends on stellar structure, with later-type stars exhibiting more efficient dissipation (smaller Q_*), and probably also on tidal driving frequency.

One way to constrain Q_* and the galactic engulfment rate for exoplanet systems would be to observe tidally driven orbital decay, which would manifest as variations in transit timing. Unfortunately, tidal decay has only been definitively detected this way for one hot Jupiter, WASP-12 b (Patra et al. 2017; Yee et al. 2020). The period decay rate reported in Yee et al. (2020) $dP/dt = -29 \pm 2 \text{ ms yr}^{-1}$ translates to $Q_* \approx 2 \times 10^5$ and amounts to a change in the period of just under half a second since the planet was discovered in 2008. A recent analysis of TESS data confirmed this decay rate, reducing the error bars below 1 ms yr^{-1} (Wong et al. 2022). Possible tidal decay has also been reported for several other systems, including for XO-3 b (Yang & Wei 2022; Ivshina & Winn 2022), WASP-19 b (Patra et al. 2020; Ivshina & Winn 2022), TrES-1 b, TrES-2 b, HAT-P-19 b (Hagey et al. 2022), Kepler-1658 b (Vissapragada et al. 2022), and KELT-9 b (Harre et al. 2023). However, definitive confirmation will likely require additional years of observations, and knowing which planets to prioritize requires understanding how decay is detected and what parameters best suit a system to exhibit detectable decay.

Detecting tidal decay requires fitting an ephemeris to observed transit times. In the absence of tidal decay, the transit times are regularly spaced (by orbital period P) and increase linearly with observational epoch E . When there is tidal decay, transits come faster and faster over time as the orbital period declines, and an additional quadratic term proportional to E^2 and involving the period change dP/dE appears in the ephemeris. Deciding whether a series of transit times is better modeled with a linear ephemeris with no decay or a quadratic ephemeris with decay requires considering more than the standard reduced χ^2 (Press et al. 2002): the quadratic ephemeris can always, in principle, result in a smaller reduced χ^2 because it involves one additional model parameter than the linear ephemeris.

In recent years, astronomers have invoked the Bayesian Information Criterion BIC (Schwarz 1978) to judge whether a dataset supports tidal decay. This simple expression incorporates both χ^2 , thereby favoring models that minimize residuals, and a term that penalizes introducing additional model parameters, thereby favoring lower-dimensional models. In this context, the BIC can be written as

$$\text{BIC} = \chi^2 + k \ln N, \quad (1)$$

where N is the total number of data points and k is the number of fit parameters, 2 for a linear fit and 3 for a quadratic fit. Generally, when comparing two models, the one with the smaller BIC is favored. For a difference in BIC between two models ΔBIC , Yee et al. (2020) pointed out that the Bayes factor, B , i.e., the ratio of posterior probabilities favoring the linear (no tidal decay) to the quadratic (tidal decay) model, is given by

$$B = \exp(-\Delta\text{BIC}/2). \quad (2)$$

As an example, the collection of transit timing observations for WASP-12 b considered here give $\Delta\text{BIC} \approx 200$, favoring a model with tidal decay by a probability $\sim 10^{43}$ times larger than a model without tidal decay. Given its utility, in this study, we explore the various system parameters and observational strategies that can promote detection of tidal decay, framing our analysis around the BIC.

We focus on the effects of tidal decay on a transiting planet's ephemeris. However, other astrophysical processes can impact it as well. Orbital precession, for example, can accelerate the transit times, thereby mimicking the effects

of tidal decay, at least as far as the transit is concerned (Patra et al. 2020). Observing a planet’s eclipse times can distinguish between decay and precession since the former will accelerate both transit and eclipse times, but the latter will accelerate one and decelerate the other. Both mechanisms, though, introduce curvature into the ephemeris (whether the transit or eclipse ephemeris), and the analysis presented here can be used to explore the detection of ephemeris curvature, whatever the cause (or sign). Future studies may better tailor this approach to searches for precession, line-of-sight acceleration (e.g., Deeg et al. 2008), or other ephemeris perturbations.

In what follows, we first explore what astrophysical properties for a planetary system best lend themselves to precise transit times (Section 2.1). Then, we consider the details of fitting both linear and quadratic curves in the cases of tidal decay and no tidal decay (Sections 2.2, 2.3, and 2.4). Finally, we apply our formulation to several hypothetical observing programs and then to real observational data for a few systems with possible tidal decay (Section 3). Throughout the analysis, we invoke the WASP-12 system as a point of comparison. Since WASP-12 is the only system with definitively detected tidal decay, the evolution over time of the various detection statistics we explore here for this system serves as a template for detecting tidal decay in other systems.

2. ANALYSIS

For our analysis, we considered data for hot Jupiter and short-period brown dwarf systems from the NASA Exoplanet Archive downloaded on 2023 Apr 5 and subject to the following requirements:

1. The planet must have “Published Confirmed” listed in the “Solution Type” column.
2. The planetary system must have listed the ratios of both the stellar radius to the semi-major axis and the planetary to stellar radius.
3. The orbital period $P < 3$ days.
4. The planet’s radius R_p lay between five times Earth’s R_{Earth} and ten times Jupiter’s R_{Jupiter} .
5. The planet has an estimated mass M_p .
6. The planet must have a published orbital period P and transit mid-point T_0 (called “Time of Conjunction” on the Exoplanet Archive), along with corresponding uncertainties.

The disintegrating planet WD 1856+534 b also happens to satisfy all these criteria, but we dropped it as irrelevant. In some cases, the most recent set of system parameters provided on the Exoplanet Archive did not include required values. In those cases, we used the most recent set of values that *did* include everything needed. In a handful of cases, we had to calculate the orbital semi-major axes from the provided period and stellar mass. These criteria left us with 137 systems.

2.1. Simplified Central Time Uncertainties

To explore the astrophysical properties that support precise transit time estimates, we start with a simplified model for the central time t_c of a transit or eclipse (Carter et al. 2008). This model involves (among other simplifications) neglecting orbital eccentricity and limb-darkening and assuming that the transiting planet is small compared to the star and that the out-of-transit baseline is very accurately estimated. (Numerical experimentation using fully accurate transit light curves shows this simplified estimate is good to about 10%.) Carter et al. (2008) defines several useful parameters related to the transit:

$$\tau_0 = \frac{R_\star}{a} \frac{P}{2\pi}, \quad (3)$$

$$b = \frac{a}{R_\star} \cos i, \quad (4)$$

$$T = 2\tau_0 \sqrt{1 - b^2}, \quad (5)$$

$$\tau = 2\tau_0 \left(\frac{R_p}{R_\star} \right) (1 - b^2)^{-1/2}, \quad (6)$$

where R_\star is the stellar radius, a is the orbital semi-major axis, P is the orbital period, i is the orbital inclination, b is the impact parameter, T is the total transit duration (defined as the time for the planet’s center to cross from limb to

limb), and τ is the ingress/egress duration. We also need a transit or eclipse depth δ

$$\delta \approx \begin{cases} \left(\frac{R_p}{R_\star}\right)^2 & \text{transit} \\ \left(\frac{R_p}{R_\star}\right)^2 \frac{I_p}{I_\star} & \text{occultation,} \end{cases} \quad (7)$$

where $I_{p/\star}$ is the planetary/stellar disk-integrated intensity (Winn 2010).

We also need the following parameters as defined in Carter et al. 2008:

$$Q = \sqrt{\Gamma T} \frac{\delta}{\sigma}, \quad (8)$$

$$\theta = \frac{\tau}{T}, \quad (9)$$

with Γ the sampling rate for the transit observations (assumed constant) and σ the per-point photometric uncertainty. Q , therefore, correlates with total signal-to-noise ratio for the transit, and θ is the ratio of the ingress/egress duration to the total transit duration. Based on these definitions, Carter et al. (2008) provide a simplified estimate for the uncertainty on the central time t_c

$$\sigma_{t_c} = TQ^{-1} \sqrt{\theta/2}. \quad (10)$$

Plugging in all the above defined parameters, we find that

$$\sigma_{t_c} = \sqrt{\frac{\tau}{2\Gamma}} \left(\frac{\sigma}{\delta}\right) = \sigma \Gamma^{-1/2} \left(\frac{R_\star}{a}\right)^{1/2} \left(\frac{P}{2\pi}\right)^{1/2} \left(\frac{R_p}{R_\star}\right)^{-3/2} (1-b^2)^{-1/4} \times \begin{cases} 1 & \text{transit} \\ \left(\frac{I_p}{I_\star}\right)^{-1} & \text{eclipse} \end{cases} \quad (11)$$

Not surprisingly, the uncertainty increases with the photometric uncertainty and decreases as the transit depth and sampling rate increase. Why, though, does the mid-transit uncertainty increase with ingress/egress duration? Consider a case with a very long ingress/egress (e.g., a near-grazing transit with $b \rightarrow 1$), which corresponds to a very nearly V-shaped light curve. In that case, determining the mid-transit time relies on being able to determine when exactly the light curve goes from decreasing with time to increasing with time, with very little transition in-between. Without sufficient sampling, for example, the instant of transition would be missed, and the mid-transit time would be highly uncertain.

Figure 1 compares estimates of transit σ_{t_c} for several systems to an estimate for WASP-12 b based on Equation 11. Although it is impossible to estimate the per-point photometric uncertainty σ for any system in general since the photometric uncertainty depends on the complex details of a particular observation, we can at least include the approximate dependence on stellar magnitude. First, we can relate the photon count rate N to the stellar flux in the bandpass of observation F as $N \propto F$. Then we can fold in the relationship between flux and apparent magnitude $m \propto -2.5 \log_{10} F$. Assuming Poisson statistics gives

$$\sigma \propto 10^{-m/5}. \quad (12)$$

Although simplified, the calculations illustrated in Figure 1 show that there are many systems that we might expect to have smaller timing uncertainties than WASP-12 b and many systems with tidal decay expected to be larger. But there are only three with both: WASP-103 b, KELT-16 b, and KELT-1 b. Barros et al. (2022) analyze combined ground- and space-based transit observations of WASP-103 b, realizing typical timing uncertainties about 50% smaller than those for WASP-12 b reported in Yee et al. (2020). However, Barros et al. (2022) report no detection of tidal decay but do see tidal deformation of the planet. Likewise, Harre et al. (2023) combine ground- and space-based data for KELT-16 b and find that the BIC favors no tidal decay but only slightly: BIC = 292.9 for a constant period and BIC = 297.6 for decay. Finally, Baştürk et al. (2023) combine 19 transit observations for the brown dwarf system KELT-1 b and also find no evidence for tidal decay but do report possible signs of tidal synchronization of the host star's rotation.

Having developed a sense for the range of timing uncertainties and tidal decay rates, we next turn to how transit observations are transformed into ephemerides, both those that include no decay (i.e., linear in the observational epoch E) and those that do include it (i.e., quadratic in E).

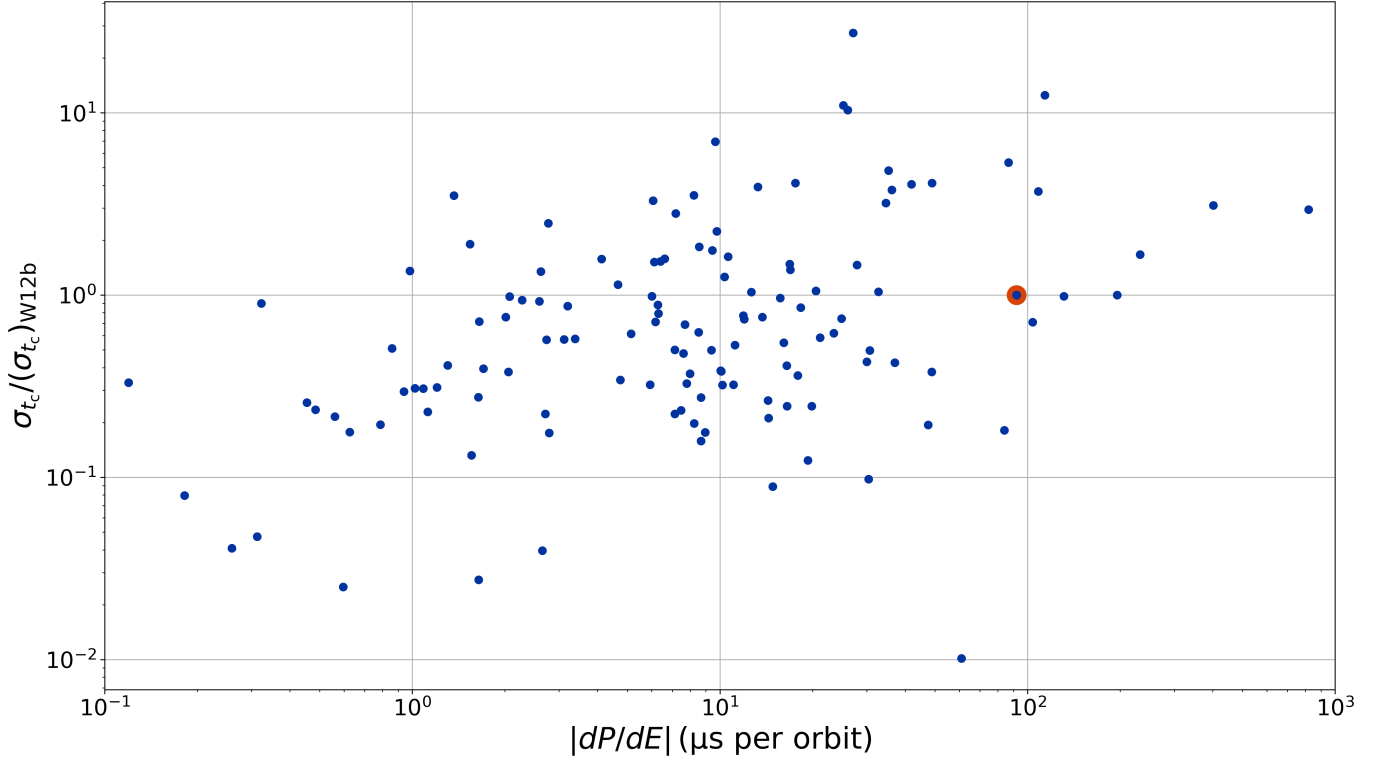


Figure 1. Simplified mid-transit time uncertainties (Equation 11) normalized to the estimate for WASP-12 b (orange marker) vs. the orbital decay (Equation 22 in Section 2.3) for many confirmed systems.

2.2. Fitting a Linear Curve to a Linear Ephemeris

For a linear fit to a linear ephemeris based solely on transits, we can calculate the uncertainties on T_0 and P using the epoch E for each observed transit and the associated mid-transit time uncertainty $\sigma_{t(E)}$. We use $\sigma_{t(E)}$ to represent the actually observed uncertainty (as opposed to the analytic uncertainty for a single transit σ_{t_c} or the uncertainty for the predicted future transit time $\sigma_{t_{\text{tra}}^{\text{pred}}}$). The predicted time and associated uncertainty for the transit time are, respectively,

$$t_{\text{tra}}^{\text{pred}} = T_0 + PE, \quad (13)$$

$$\sigma_{t_{\text{tra}}^{\text{pred}}} = \sqrt{\sigma_{T_0}^2 + E^2\sigma_P^2 + 2E\sigma_{T_0,P}} \approx \sqrt{\sigma_{T_0}^2 + E^2\sigma_P^2}, \quad (14)$$

Although the $\sigma_{T_0,P}$ term contributes, in practice, it is usually orders of magnitude smaller than the other terms, so we neglect it.

We can estimate the uncertainties analytically using standard linear regression (cf. Press et al. 2002). First, define

$$\begin{aligned} S &= \sum_{E \in \text{transits}} \left(1/\sigma_{t(E)}^2 \right) \\ S_E &= \sum_{E \in \text{transits}} \left(E/\sigma_{t(E)}^2 \right) \\ S_{E^2} &= \sum_{E \in \text{transits}} \left(E^2/\sigma_{t(E)}^2 \right). \end{aligned} \quad (15)$$

Then

$$\sigma_{T_0}^2 = \frac{S_{E^2}}{SS_{E^2} - (S_E)^2} \quad (16)$$

$$\sigma_P^2 = \frac{S}{SS_{E^2} - (S_E)^2}. \quad (17)$$

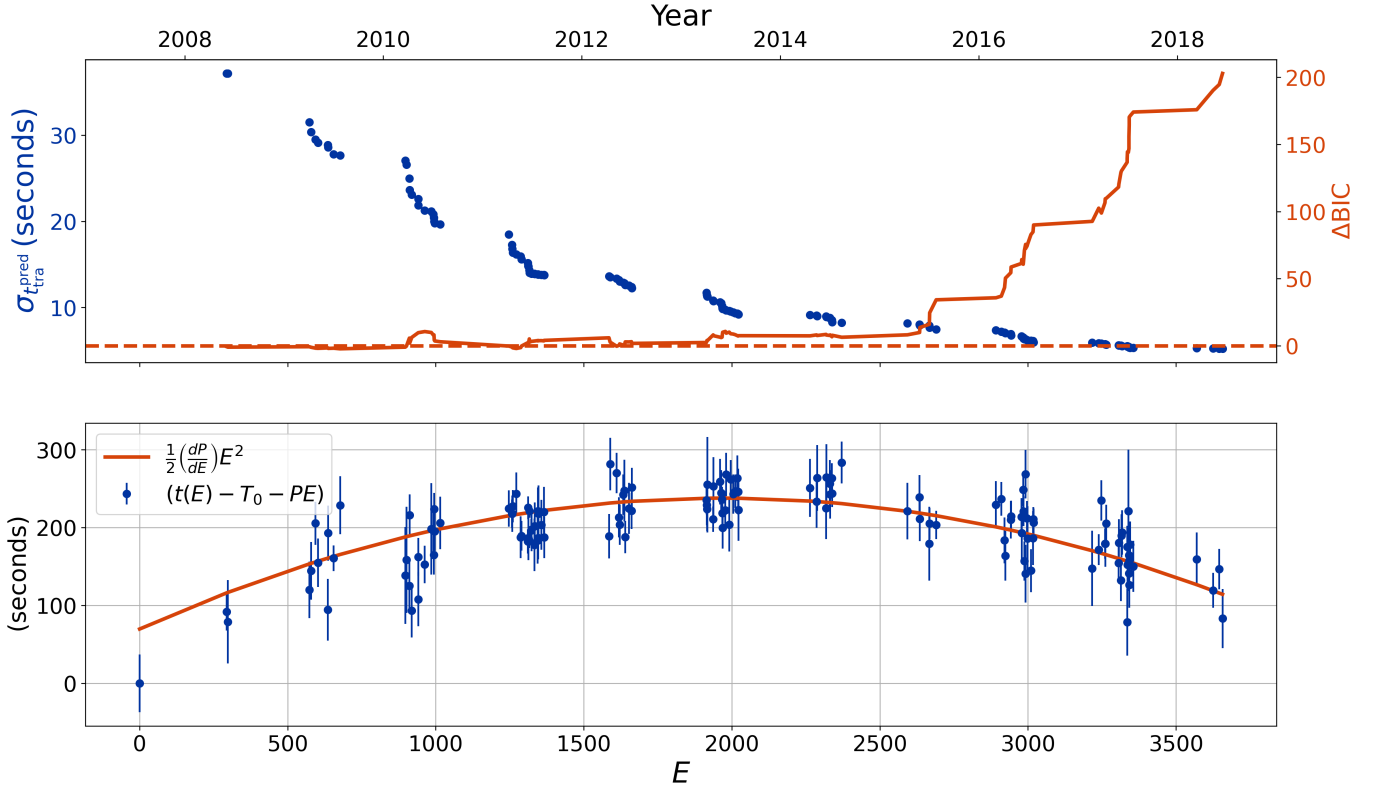


Figure 2. (top) The blue dots show the evolution of $\sigma_{t_{\text{tra}}^{\text{pred}}}$ for WASP-12 b during the last several years, as calculated using the data from Yee et al. (2020) and Equation 14. The orange curve (which uses the right y-axis) illustrates the corresponding evolution of the difference in Bayesian Information Criterion (BIC) comparing a linear ephemeris BIC(lin) to a quadratic ephemeris BIC(quad). (bottom) The blue dots show the difference between the observed transit time $t(E)$ at epoch E and a linear ephemeris fit $T_0 + PE$. The orange line shows the quadratic ephemeris term using the dP/dE ($86.7 \mu\text{s orbit}^{-1}$) from Yee et al. (2020).

Figure 2 illustrates how adding more and more observations impacts $\sigma_{t_{\text{tra}}^{\text{pred}}}$ by following the history of transit observations of WASP-12 b.

Of course, if we wait for a while before observing another transit, the uncertainty for the next expected transit time will grow as in Equation 14. If we waited long enough t_{wait} that $\sigma_{t_{\text{tra}}^{\text{pred}}}$ grows beyond some value, then scheduling the next transit observation could be challenging:

$$t_{\text{wait}} = \sqrt{\sigma_{t_{\text{tra}}^{\text{pred}}}^2 - \sigma_{T_0}^2} \left(\frac{P}{\sigma_P} \right). \quad (18)$$

Systems that have not been observed for t_{wait} are the ones for which additional transit observations would be most fruitful for improving the linear ephemeris. For the systems considered here, Figure 3 shows the expected time we would have to wait for $\sigma_{t_{\text{tra}}^{\text{pred}}}$ to grow as large as the transit duration T since the T_0 value reported on the Exoplanet Archive (as of 2023 Apr 5). Most planets have sufficiently precise linear ephemerides that we would have to wait many years before uncertainties on their expected $t_{\text{tra}}^{\text{pred}}$ grew as large as their transit durations, but uncertainties for a handful are likely large enough to warrant follow-up already, at least based on the Exoplanet Archive data. CoRoT-14 b, for example, has an orbital period $P = 1.51214 \pm 0.00013$ days and $T_0 = 2454787.6702 \pm 0.0053$ JD (Bonomo et al. 2017), which corresponds to 2008 Nov. Over the last decade and a half, $\sigma_{t_{\text{tra}}^{\text{pred}}}$ has grown as large as its transit duration, $T = 1.2$ hours. Very near the one-to-one line, WASP-103 b was recently observed by the CHEOPS telescope, observations which actually suggest an orbital period increase rather than a decrease (Barros et al. 2022). However, the resulting ephemeris was too recent to have been included in our data, and so we do not consider it here. TrES-3 b is a similar case – we did not use more recent observations (e.g., Mannaday et al. 2022) that would likely update

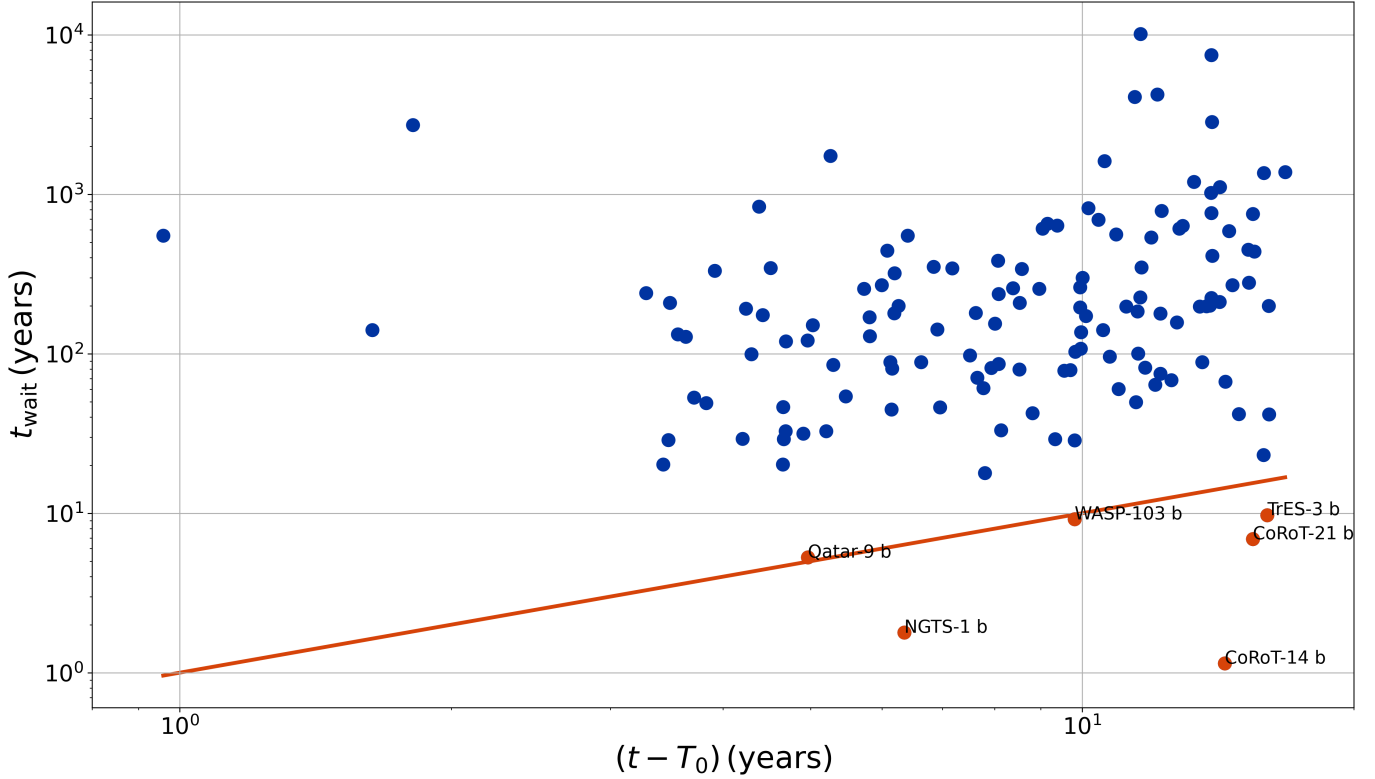


Figure 3. The time t_{wait} expected before the uncertainty on the linear ephemeris $\sigma_{t_{\text{tra}}^{\text{pred}}}$ (Equation 14) grows as large as the transit duration T vs. the time (as of 2023 Apr 5) since the T_0 value reported on the Exoplanet Archive. The orange line shows $y = x$, and the orange points are systems which lie near or below that line. For these systems, additional transit observations would likely significantly improve the linear ephemeris.

its timing uncertainty and increase t_{wait} . Determining whether individual systems require follow-up or just updated ephemerides, we leave for future work.

Finally, fitting a linear curve to a linear ephemeris would be expected to result in a BIC given by

$$\text{BIC}(\text{lin}) = (N - 2) + 2 \ln N. \quad (19)$$

2.3. Fitting a Quadratic Curve to a Quadratic Ephemeris

For a quadratic ephemeris, the predicted time and associated uncertainty for the time of the E th transit are, respectively,

$$t_{\text{tra}}^{\text{pred}} = T_0 + PE + \frac{1}{2} \left(\frac{dP}{dE} \right) E^2, \quad (20)$$

$$\sigma_{t_{\text{tra}}^{\text{pred}}} \approx \sqrt{\sigma_{T_0}^2 + E^2 \sigma_P^2 + \frac{1}{4} E^4 \sigma_{dP/dE}^2}, \quad (21)$$

where we have again neglected covariance between fit parameters.

For tidal decay involving a constant phase lag (i.e., a constant value for the star's modified tidal dissipation parameter Q_*), dP/dE is given by

$$\frac{dP}{dE} = P \frac{dP}{dt} \approx - (26 \mu\text{s per orbit}) \left(\frac{M_p}{M_{\text{Jup}}} \right) \left(\frac{M_\star}{M_\odot} \right)^{-8/3} \left(\frac{R_\star}{R_\odot} \right)^5 \left(\frac{P}{\text{day}} \right)^{-10/3} \left(\frac{Q_\star}{10^5} \right)^{-1}, \quad (22)$$

where M_p is planetary mass in Jupiter masses ($M_{\text{Jup}} = 1.89813 \times 10^{27}$ kg), M_\star is stellar mass in solar masses ($M_\odot = 1.989 \times 10^{30}$ kg), R_\star is stellar radius in solar radii ($R_\odot = 6.957 \times 10^8$ m), and P is orbital period in days.

Figure 1 compares estimates of dP/dE for many systems to dP/dE for WASP-12, assuming a WASP-12-like $Q_\star = 2 \times 10^5$. Interestingly, many systems might be expected to exhibit faster tidal decay, and many more systems likely have properties that give rise to more precise transit timing σ_{t_c} , at least based on the simplified analytic treatment outlined in Section 2.1.

By analogy with the linear case, we can analytically calculate the uncertainties on the fit parameters. For this calculation, we define

$$\begin{aligned} S_{E^3} &= \sum_{E \in \text{transits}} \left(E^3 / \sigma_{t(E)}^2 \right), \\ S_{E^4} &= \sum_{E \in \text{transits}} \left(E^4 / \sigma_{t(E)}^2 \right). \end{aligned} \quad (23)$$

With these definitions,

$$\sigma_{T_0}^2 = \frac{S_{E^3}^2 - S_{E^2} S_{E^4}}{\Delta}, \quad (24)$$

$$\sigma_P^2 = \frac{S_{E^2}^2 - S S_{E^4}}{\Delta}, \quad (25)$$

$$\sigma_{dP/dE}^2 = \frac{S_E^2 - S S_{E^2}}{\Delta} \quad (26)$$

where

$$\Delta = -S S_{E^2} S_{E^4} + S S_{E^3}^2 + S_E^2 S_{E^4} - 2 S_E S_{E^2} S_{E^3} + S_{E^2}^3.$$

Fitting a quadratic curve to a quadratic ephemeris would be expected to result in

$$\text{BIC}(\text{quad}) = (N - 3) + 3 \ln N. \quad (27)$$

We can use these expressions to explore how evidence for tidal decay in the WASP-12 system mounted over the years as a template for finding other systems exhibiting tidal decay. The blue dots in Figure 4 shows the evolution of the tidal decay signal-to-noise SNR for WASP-12 b alongside the comparison of the BIC for linear and quadratic fits, $\Delta\text{BIC} \equiv \text{BIC}(\text{lin}) - \text{BIC}(\text{quad})$. ΔBIC will grow as the data favor tidal decay. Not surprisingly, as the tidal decay SNR goes up, the BIC preference for the quadratic fit increases, too.

Another requirement for observational constraints on dP/dE to be meaningful is that uncertainties on the linear portion of the ephemeris need to be small compared to the quadratic portion. Otherwise, apparent deviations from a putative linear ephemeris due to tidal decay could be attributed to the uncertainties on the linear ephemeris. This condition translates to

$$\sigma_{\text{lin}} \equiv \sqrt{\sigma_{T_0}^2 + E^2 \sigma_P^2} < \frac{1}{2} \left| \frac{dP}{dE} \right| E^2. \quad (28)$$

Figure 4 shows how this condition played out for WASP-12 b. The increase in ΔBIC clearly correlates with the growth of the quadratic term in Equation 28.

Considering other systems, Figure 5 shows the cumulative change in orbital period expected due to tidal decay for our collection of systems as compared to the uncertainty on the linear ephemeris. Systems satisfying Inequality 28 appear above the orange line. For example, WASP-12, the only system for which tidal decay has been definitively observed, appears above that line, along with several other systems. Several caveats should be considered in evaluating these results, including the fact that we have assumed $Q_\star = 2 \times 10^5$. This is the value inferred for WASP-12, which may exhibit unusually efficient tidal dissipation (Weinberg et al. 2017) and therefore may not be a representative value. For some well-observed systems, such as WASP-18b and WASP-19b, the lack of observed orbital decay to date has been used to constrain their values of Q_\star to $> 10^7$ and $> 10^6$, respectively (Rosário et al. 2022). Even so, the results point to several systems that merit follow-up transit observations. Several of the systems above the line in Figure 5 have been noted to exhibit period changes. HAT-P-23, for example, has $\frac{1}{2} \left(\frac{dP}{dE} \right) E^2 = -0.003$ days and $\sigma_{\text{lin}} = 0.002$ days, while Hagey et al. (2022) reported $dP/dt = -5.2 \pm 5.8$ ms yr⁻¹ (which works out to $\Delta P \approx -0.004$ days since T_0 for HAT-P-23 b).

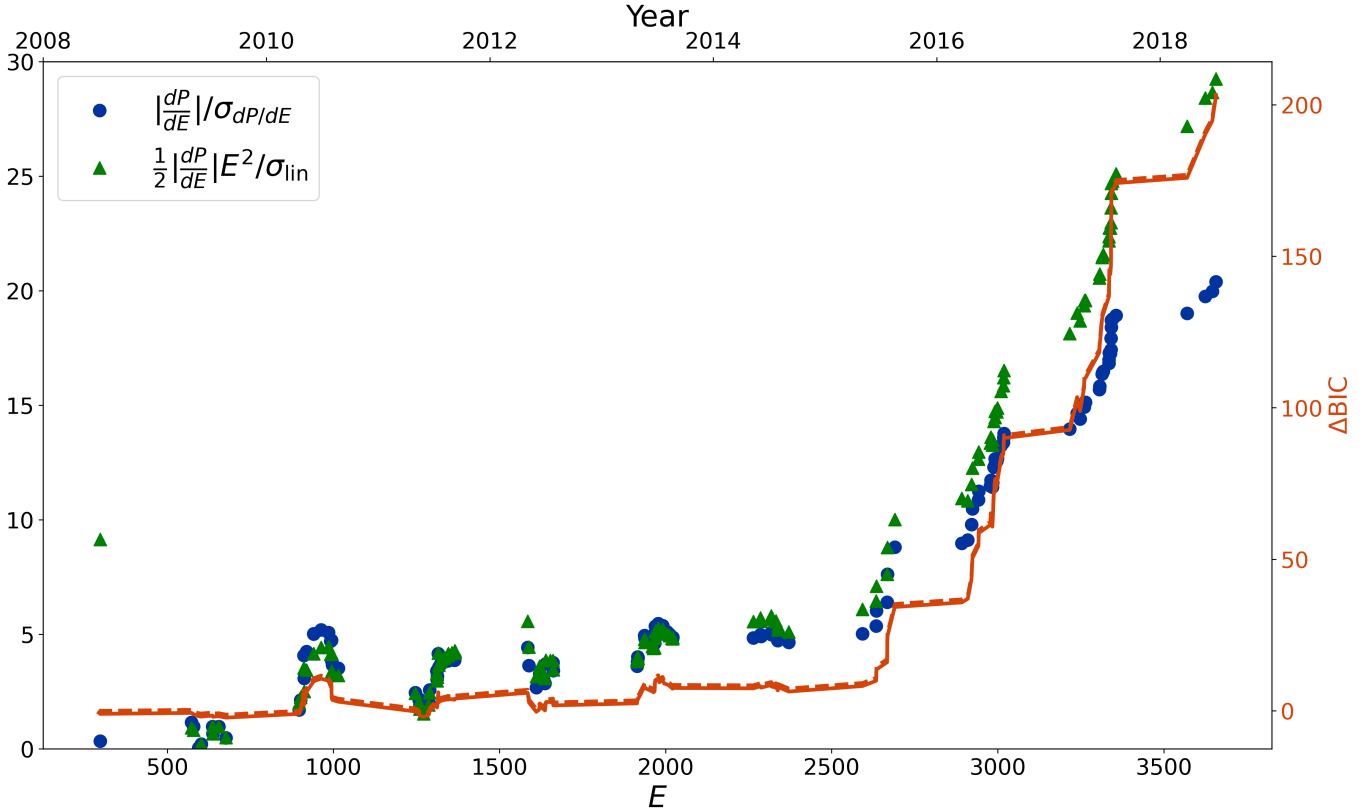


Figure 4. The blue dots show the evolution of the tidal decay signal-to-noise $\text{SNR} = |dP/dE|/\sigma_{dP/dE}$ for WASP-12. The green triangles show the corresponding evolution of the best-fit quadratic term $\frac{1}{2}|dP/dE|E^2/\sigma_{\text{lin}}$. Both of these data use the left y-axis. The orange curve shows the same difference in BIC values as shown in Figure 2 calculated numerically. These results are based on the same data as in Figure 2 and as reported in Yee et al. (2020). The dashed orange line shows the analytic approximation given by Equation 34.

2.4. Fitting a Linear Curve to a Quadratic Ephemeris

Finally, we consider the case of fitting a linear curve to a quadratic ephemeris. Analyzing this case is useful since it will allow us to explore how to estimate the BIC thresholds we should look for if we suspect a planet shows signs of tidal decay. (The other combination, fitting a quadratic to a linear ephemeris, would, in principle, result in a quadratic coefficient statistically consistent with zero and the same BIC expression as from Section 2.3.)

To start, consider the linear curve that results from fitting the quadratic ephemeris. Since $|dP/dE| \ll T_0$ and $|dP/dE| \ll P$ (where T_0 and P are the true values for the system), we might suspect that the best-fit values, which we will call T'_0 and P' , would closely resemble the actual values, i.e. $T'_0 \approx T_0$ and $P' \approx P$. Indeed, fitting a linear curve to the transit times for WASP-12 b from Yee et al. (2020) returns T'_0 and P' that match T_0 and P to better than a few parts in ten thousand. But the large collection of high quality data for WASP-12 b means that even this small disagreement is still statistically discrepant. This result comports with the results from Section 2.3: those systems for which we have sufficient data to detect a non-zero dP/dE are also those for which we have very small error bars on T_0 and P . Therefore, in order to calculate BIC for fitting a linear curve to a quadratic ephemeris, we will need also to calculate T'_0 and P' , which can be written as

$$T'_0 = T_0 + \left(\frac{dP}{dE}\right) \Delta T'_0 \quad (29)$$

$$P' = P + \left(\frac{dP}{dE}\right) \Delta P'. \quad (30)$$

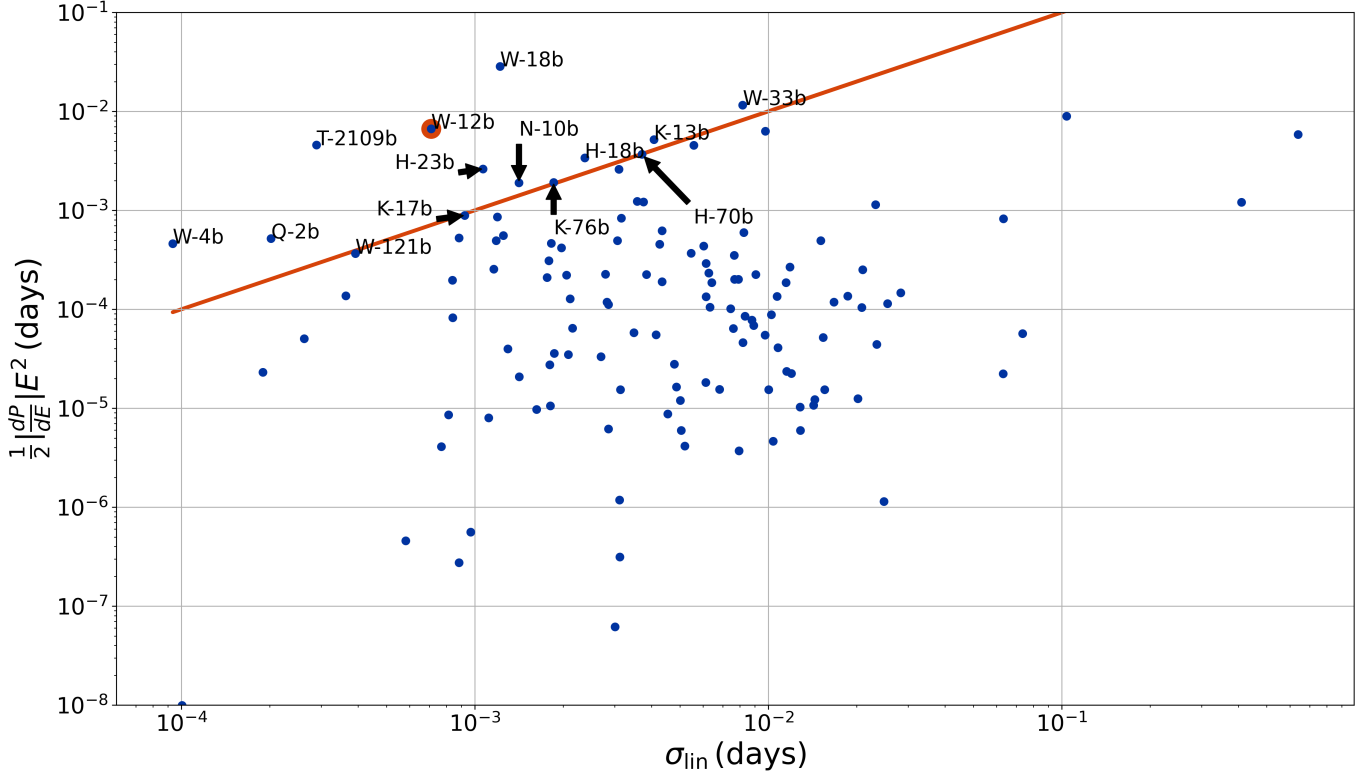


Figure 5. Cumulative change in orbital period due to tidal decay expected theoretically vs. uncertainties on the linear ephemeris (Equation 14). WASP-12 b is shown with an orange circle, and the orange line shows $y = x$. Systems above that line may have experienced sufficient tidal decay since T_0 that it is distinguishable from uncertainties on the linear ephemeris. Individual planets near or above the line are labeled as follows: HAT-P-23 b = “H-23b”, HATS-18 b = “H-18b”, HATS-70 b = “H-70b”, KOI-13 b = “K-13b”, Kepler-17 b = “K-17b”, Kepler-76 b = “K-76b”, NGTS-10 b = “N-10b”, Qatar-2 b = “Q-2b”, TOI-2109 b = “T-2109b”, WASP-12 b = “W-12b”, WASP-121 b = “W-121b”, WASP-18 b = “W-18b”, WASP-33 b = “W-33b”, WASP-4 b = “W-4b”.

where $\Delta T'_0$ and $\Delta P'$ are the corrections we need to work out. As outlined in the Appendix, standard linear regression gives the following formulae for $\Delta T'_0$ and $\Delta P'$:

$$\Delta T'_0 = \left(\frac{S_{E^2}^2 - S_{E^3} S_E}{S_{E^2} S - S_E^2} \right) \quad (31)$$

$$\Delta P' = \left(\frac{S_{E^3} S - S_{E^2} S_E}{S_{E^2} S - S_E^2} \right). \quad (32)$$

Now, we can calculate the resulting χ^2 for fitting a linear curve to a quadratic ephemeris:

$$\begin{aligned} \chi^2 &= \sum_{E \in \text{transits}} \left(\frac{t(E) - P'E - T'_0}{\sigma_{t(E)}} \right)^2 \\ &\approx \frac{1}{4} \left(\frac{dP}{dE} \right)^2 \sum_{E \in \text{transits}} \left(\frac{E^2 - \Delta P'E - \Delta T'_0}{\sigma_{t(E)}} \right)^2 + (N - 2) \end{aligned} \quad (33)$$

and the difference in BIC values for a linear curve and a quadratic curve, both fit to a quadratic ephemeris as determined analytically

$$\Delta \text{BIC} = \frac{1}{4} \left(\frac{dP}{dE} \right)^2 \sum_{E \in \text{transits}} \left(\frac{E^2 - \Delta P'E - \Delta T'_0}{\sigma_{t(E)}} \right)^2 - \ln N + 1. \quad (34)$$

Of course, given a set of already observed transits, we could easily calculate the ΔBIC . The benefit of Equation 34 is that we can estimate the ΔBIC expected for a sequence of *planned* transit observations that have yet to be conducted

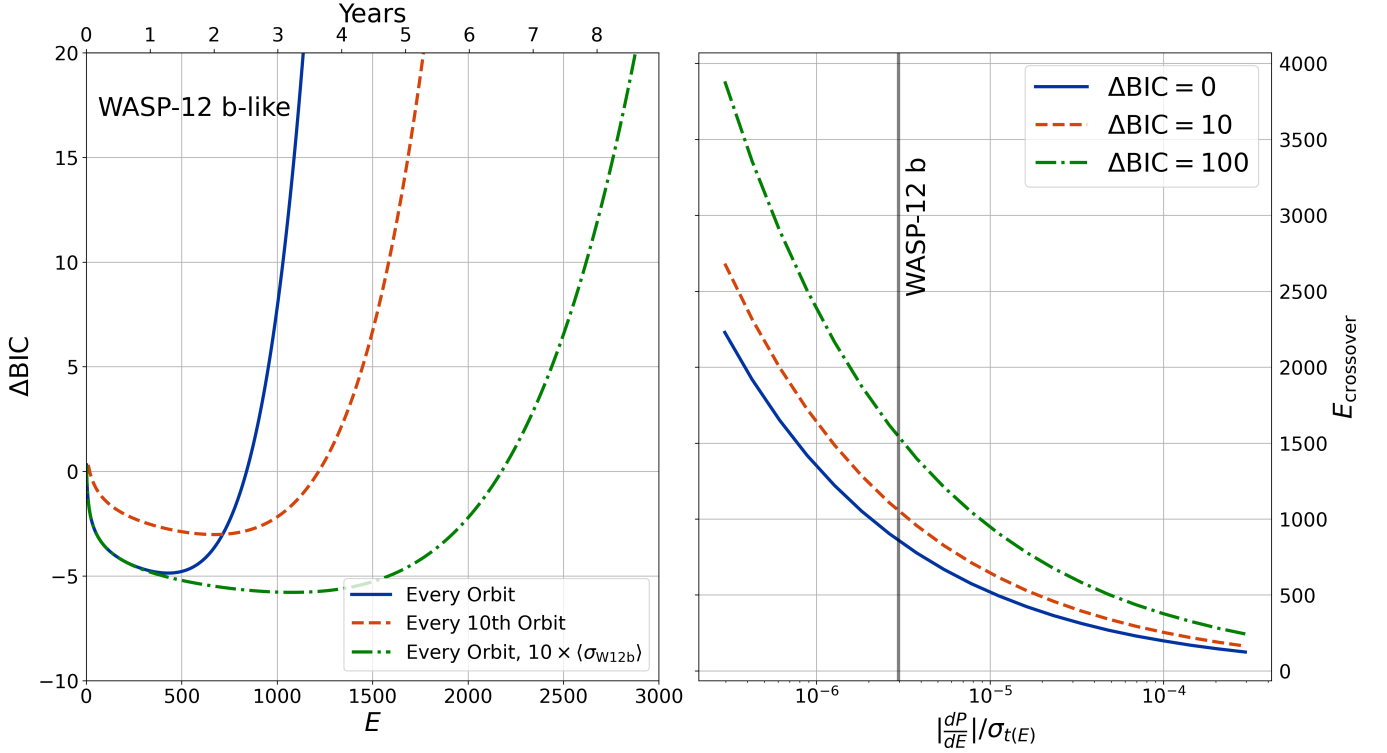


Figure 6. Application of Equation 34 to planetary systems with WASP-12 b-like tidal decay and transit-timing uncertainties. The left panel shows the evolution of ΔBIC assuming (1) a transit is observed every orbit (solid blue curve), (2) a transit is observed every tenth orbit (dashed orange), and (3) a transit is observed every orbit but with a timing uncertainty ten times larger than the other two cases (dash-dot green). The right panel shows the epoch $E_{\text{crossover}}$ at which ΔBIC crosses over a given value as a function of the tidal decay rate (dP/dE) and transit timing uncertainty $\sigma_{t(E)}$. As a point of comparison, for WASP-12 b, $|dP/dE|/\sigma_{t(E)} \approx 3 \times 10^{-6}$, as shown by the vertical gray line. These curves assume optimistically that the transit for every epoch is observed up to $E_{\text{crossover}}$.

(given reasonable estimates for the expected timing uncertainties). The dashed orange line in Figure 4 shows how closely the analytic approximation matches the numerical result obtained by directly comparing a linear to a quadratic fit.

3. APPLYING THE ΔBIC EXPRESSION

Applying Equation 34 to the ephemerides for transiting planets can provide the likelihood of detecting tidal decay for a given planned series of transit campaigns: for an expected tidal decay rate (Equation 22), when should observations be collected and how many? A comprehensive application of Equation 34 to the suite of transiting hot Jupiters could be fruitful in these ways, but for the present paper, we confine our application to a few example cases.

3.1. Hypothetical Cases

First, we consider hypothetical cases to gauge how effectively tidal decay could, in principle, be detected by various observing strategies for planetary systems with definite quadratic ephemerides. For many of the calculations in this section, we assumed a tidal decay rate equal to WASP-12 b's, $P/|dP/dt| = 2.3 \text{ Myrs}$ or $dP/dE = 86.7 \mu\text{s orbit}^{-1}$ (Yee et al. 2020) and a constant transit timing uncertainty, $\sigma_{t(E)} = \text{const.}$ Strictly, ΔBIC depends on transit epoch E and *not* on orbital period, but to give a sense for the timescales over which observational campaigns might be conducted, we assumed WASP-12 b's orbital period $P = 1.091419649 \text{ days}$ to convert from E to years.

To begin with, we consider some overly simple observational campaigns – left panel of Figure 6. (N.B.: Throughout this section, the x- and y-axes of different panels often do *not* match up.) For the blue and orange lines, that uncertainty was taken as equal to the median for the WASP-12 b dataset from Yee et al. (2020), $\sigma_{t(E)} = \langle \sigma_{\text{W12b}} \rangle = 0.00032 \text{ days}$, while the green line shows the result for an uncertainty ten times larger (0.0032 days). The blue and green lines show

how ΔBIC would grow if we could (unrealistically) observe every transit, while the orange line shows what would happen if we observed every tenth transit.

As previously stated, $\Delta\text{BIC} > 0$ indicates a statistical preference for a quadratic over a linear ephemeris, and all curves in the left panel of Figure 6 show ΔBIC initially drop from zero into negative values. Intuitively, this behavior reflects the need for curvature in the ephemeris to build up over time so that the quadratic term ($\frac{1}{2}|dP/dE|E^2$ – see Equation 20) grows sufficiently large that a linear regression is impacted. In other words, we have to wait for a while after a transiting planet is discovered to spot tidal decay. Equation 34 indicates that that crossover point depends on the total number of observations N , the timing/frequency of those observations (the summation term), the timing uncertainty, and the tidal decay rate dP/dE .

The right panel of Figure 6 shows the dependence of the crossover epoch $E_{\text{crossover}}$ for a desired ΔBIC value on the ratio $|dP/dE|/\sigma_{t(E)}$, assuming every transit since a planet’s discovery is observed. If, for example, $\Delta\text{BIC} = 10$ were the goal of an observing program (dashed, orange curve) for a system with WASP-12 b-like properties ($|dP/dE|/\sigma_{t(E)} \approx 3 \times 10^{-6}$), then a minimum of about 1000 transits would need to be observed. Approaching the situation from the opposite direction, a survey including nearly every single transit up to $E = 1500$ and with WASP-12 b-like timing uncertainties would be expected to achieve $\Delta\text{BIC} \approx 100$ if the system actually exhibited WASP-12 b’s tidal decay. In this way, we can apply Equation 34 to a particular observing program to determine a reasonable threshold for decay detection.

Consider next somewhat more realistic observing campaigns – Figure 7. The top left panel compares ΔBIC growth for one transit observation and two observations in one Earth year. In about nine Earth years, the curve corresponding to twice annual observations (dashed orange) has grown to nearly twice the ΔBIC for once annual observations (solid blue). The top right panel compares ΔBIC growth for one observation every two months all Earth year-round and the other involving one observation every two months for six months (dashed orange). Here, the two curves weave over one another, suggesting little advantage of one program over the other. This result is not surprising since little curvature develops in the ephemeris over six months.

Next, consider the bottom left panel of Figure 7. The solid blue curve involves two consecutive transit observations each Earth year, while the dashed orange curve involves ten consecutive observations each Earth year. Not surprisingly, ΔBIC increases much more rapidly for the latter program than for the former since, in each observing session, significantly more transits are collected. The dash-dot green curve involves the same total number of transits as the dashed, orange curve but randomly phased (i.e., not necessarily consecutive transits), illustrating that the timing of observations over a short (compared to the decay time) timescale has minimal impact on the evolution. For this particular instantiation, the final ΔBIC ends up slightly below the dashed, orange curve, but other examples (not shown) have ΔBIC equal to or even slightly above the dashed, orange curve, depending on exactly how the observations are timed.

Finally, consider the bottom right panel of Figure 7. This panel shows how ground-based observations can combine with observations from a TESS-like mission to detect tidal decay. For this calculation, we first assumed every transit was observed for a WASP-12-like system during a 27-day period in each year, followed by no observations for 25 TESS sectors, and then another sequence of transits were observed, etc. The solid blue line shows this scenario. The dashed orange line shows the same program except with a single ground-based transit included every six months. The dash-dot, green line shows the same program except with six ground-based transit observations, randomly spread during a six-month observing season. Not surprisingly, ΔBIC for the TESS + ground programs grows more quickly, demonstrating the power of combining the two approaches. The dash-dot green line (six ground-based transits) modestly significantly exceeds the solid blue line once the signal of tidal decay starts to emerge and ΔBIC grows large, while the dotted orange line (one ground-based transit) only modestly exceeds it.

Although the approach here needs to be tailored to each specific observing program for detailed predictions, these results illustrate its general utility. They show that detecting tidal decay requires collecting regular observations and allowing sufficient time for decay to manifest. In general, a significant increase in ΔBIC requires a significant fractional increase in the number of observations. Adding just a few more observations to an already full observing program does not make much difference unless they are judiciously timed. Two encouraging conclusions of these results: (1) an observing program that can only observe a few times a year can still have an impact, and (2) it may be more worthwhile to double the number of candidates, focusing on the planets most likely to exhibit decay, than to double the number of transits observed for a given planet if a program already involves several observations in a year.

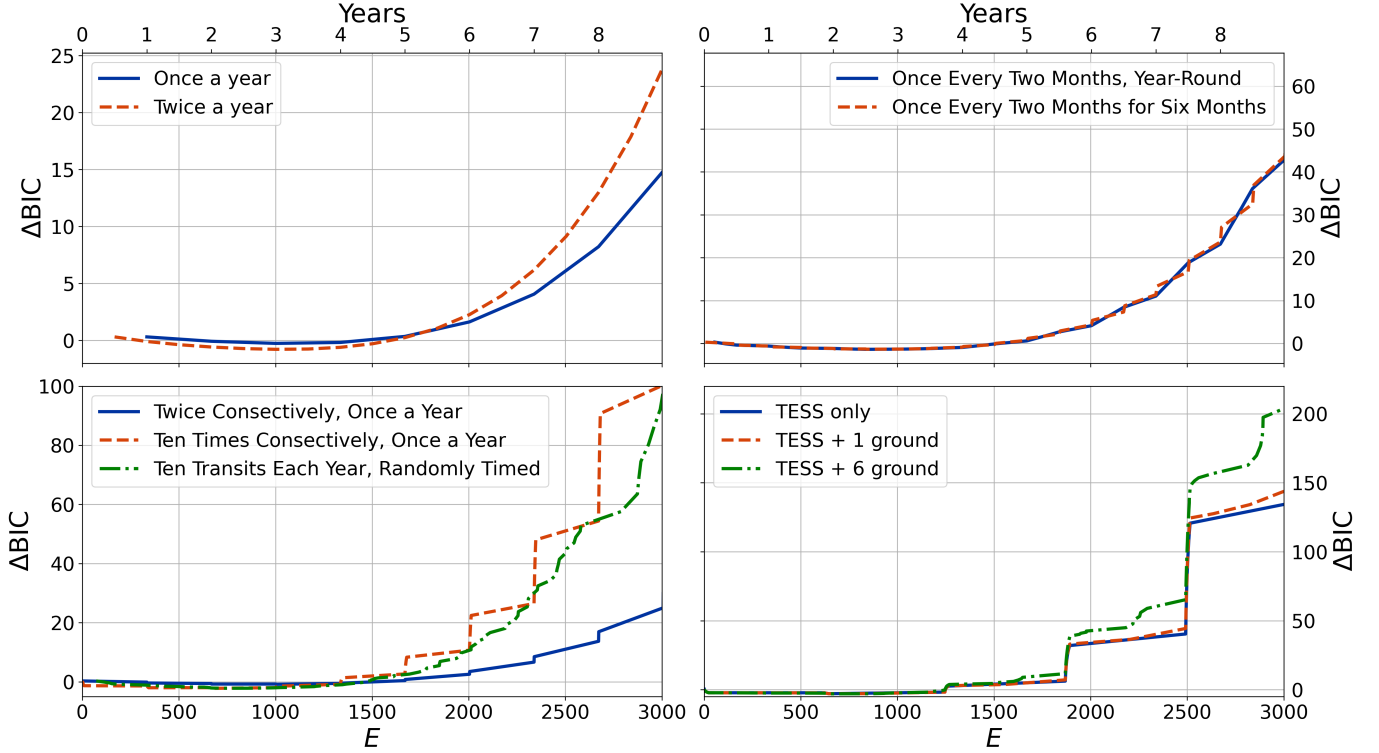


Figure 7. Application of Equation 34 to planetary systems with WASP-12 b-like tidal decay and transit-timing uncertainties using more realistic observing strategies. The top left panel shows how ΔBIC grows with one or two transit observations in an Earth year. The top right panel shows how ΔBIC grows with bi-monthly transit observations during a whole (Earth) year (solid blue curve) and during an hypothetical observing season of six months with no observations during the other six months. The bottom left panel shows how ΔBIC grows assuming two consecutive transit observations each Earth year (dashed orange curve) and ten consecutive observations each Earth year (solid blue curve). The dash-dot green curve shows the same total number of transits (ten annually) as the dashed, orange curve but randomly timed. The bottom right panel shows how ΔBIC evolves for an observational program meant to mimic TESS observations (solid blue - “TESS only”). That program involves about two dozen transits once every 25 TESS sectors, which span 27 days each. The dashed orange line (“TESS + ground”) shows the same observing program but with the addition of one transit observation every six months, meant to represent a ground-based observation. Observations for both programs assume the same transit timing uncertainties.

3.2. Real Cases

Finally, we consider real systems – Figure 8. These examples all involve systems for which possible tidal decay has been reported. We take observations for TrES-1 b, TrES-2 b, and HAT-P-19 b from Hagey et al. (2022) and observations for KELT-9 b from Harre et al. (2023). For the calculations in this section, we take the correct (and variable) transit timing uncertainties and the corresponding orbital periods to convert epoch E to (Earth) years. To extrapolate the ΔBIC evolution forward in time, we assume that observations continue with the same median frequency as before. For example, TrES-2 b has been observed every four orbits, and so we assume that same observing cadence going on past 2020.

Hagey et al. (2022) analyzed transit times reported on the Exoplanet Transit Database¹ and, for TrES-1 b, a tidal decay rate $dP/dt = -10.9 \pm 2.1 \text{ ms yr}^{-1}$ was favored over a constant period by $\Delta\text{BIC} = 9.7$. The left panel of Figure 8 shows a good match between the numerical and analytic estimates for ΔBIC , and, assuming the nominal tidal decay rate, the analytic estimate suggests ΔBIC ought to exceed 50 within the next few years. However, it may take until about 2030 to reach the same level as reported for WASP-12 b in Yee et al. (2020) – not surprising, given that WASP-12 b’s dP/dt is about twice as large.

¹ <http://var2.astro.cz/ETD/>

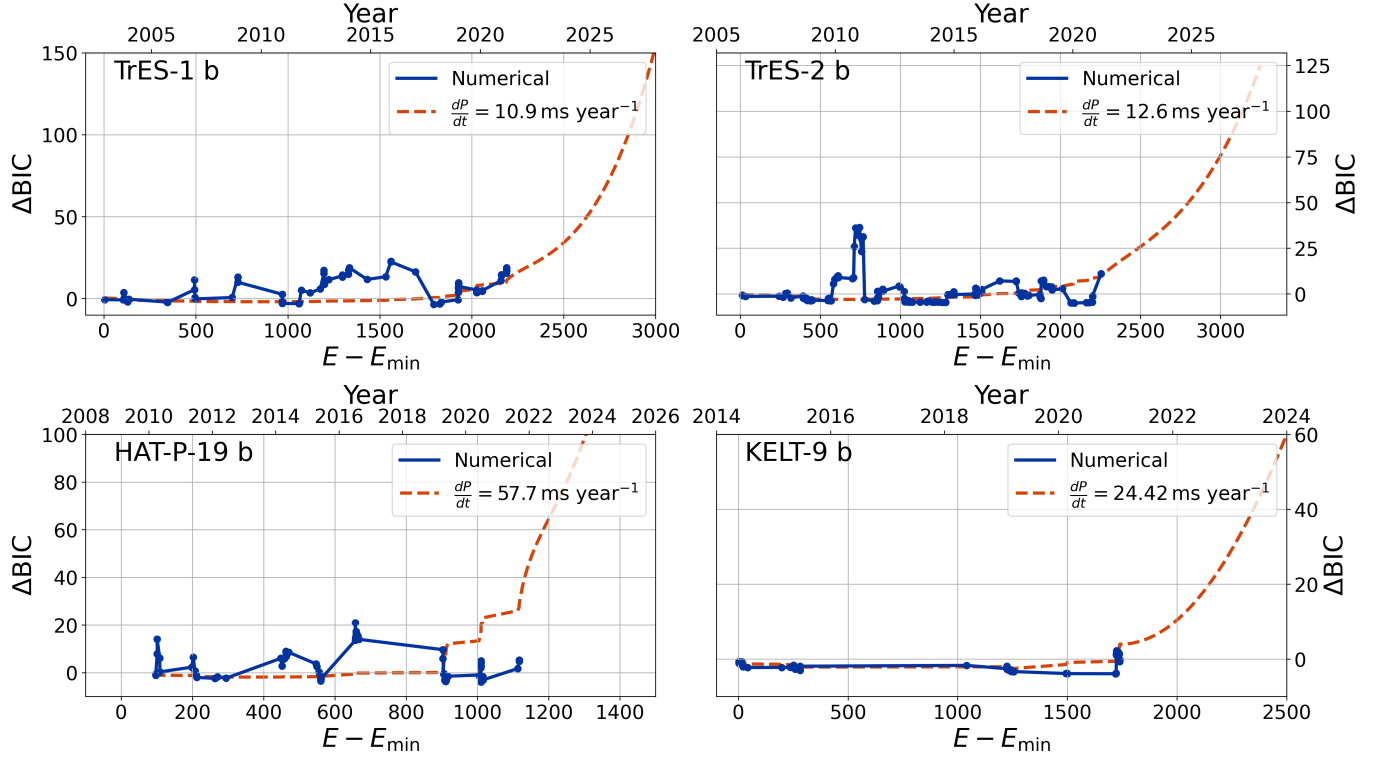


Figure 8. Evolution of ΔBIC for several real planets. The solid blue “Numerical” lines show the evolution based on previously published observations, while the dashed orange lines show the evolution based on Equation 34. For points in that latter calculation beyond the previously published observations, we assumed $\sigma_{t(E)}$ equal to the average uncertainty for the previously published observations. We also assumed the transits were observed at a cadence equal to the median cadence for the previously published observations. For example, previous transit observations of TrES-2 b have been conducted typically once every four orbits. Observations for TrES-1 b, TrES-2 b, and HAT-P-19 b come from Hagey et al. (2022), and observations for KELT-9 b come from Harre et al. (2023). For this plot, we have subtracted the minimum reported epoch E_{\min} from E .

Moving next to TrES-2 b, Hagey et al. (2022) estimated $dP/dt = -12.6 \pm 2.4 \text{ ms yr}^{-1}$ with tidal decay favored at $\Delta\text{BIC} = 8.3$. Again, Figure 8 shows a good match between the numerical and analytic estimates (albeit with considerable scatter in the “Numerical” estimate). Again, the smaller dP/dt than WASP-12 b’s means ΔBIC grows more slowly and may not exceed 50 until 2025. Like the TrES-1 data, the TrES-2 observational data show significant statistical fluctuations in ΔBIC – between $E - E_{\min} = 500$ and 1000, ΔBIC climbed rapidly before settling back toward zero. The dashed, orange line shows that such a rapid increase would not have been expected so soon after the planet’s discovery. It remains to be seen whether the recent upward tick in ΔBIC seen in the most recent data represents the beginning of true increase or whether it too is another statistical fluctuation, although the upward tick is consistent with expectations.

For HAT-P-19 b, Hagey et al. (2022) reported $dP/dt = -55.2 \pm 7.2 \text{ ms yr}^{-1}$ and $dP/dE = 606 \mu\text{s orbit}^{-1}$, with tidal decay favored at $\Delta\text{BIC} = 8.3$. This dP/dE value is almost seven times that for WASP-12 b, and the analytic ΔBIC reflects this, with a value predicted to exceed that for WASP-12 b by 2024. However, the “Numerical” estimate shows considerable non-monotonicity, reversing direction and sign several times during the observational baseline. The “Numerical” ΔBIC appears to significantly under-perform the analytic estimate. In this context, the right panel of Figure 6 is particularly useful. The average timing uncertainty for the HAT-P-19 b data is 0.0007296 days, about twice the average for WASP-12 b (0.00032 days). If all orbits since discovery had been observed, by $E - E_{\min} = 1000$, we would expect ΔBIC to exceed 100 (dash-dot green line in the right panel of Figure 6). Of course, not every orbit of HAT-P-19 b has been observed, but the fact that the “Numerical” ΔBIC does not yet exceed 10 suggests that perhaps the tidal decay reported for HAT-P-19 b is spurious.

Finally, Harre et al. (2023) combined ground-based, Spitzer, TESS, and CHEOPS transits and eclipses of the ultra-hot Jupiter KELT-9 b, which orbits a star at the A/B stellar type boundary, and reported a possible decay rate

$dP/dt = -24.42 \pm 10.66 \text{ ms yr}^{-1}$ with $\Delta\text{BIC} = 8.4$ (although the data show a preference, $\Delta\text{BIC} = 13.2$, for apsidal precession). Figure 8 shows the “Numerical” ΔBIC only became positive with the most recent observations before nosing back to 0 with the very last observation. The analytic curve suggests ΔBIC would not have been expected to cross zero until recently anyway and that it might surpass 20 in 2023. Ivshina & Winn (2022) also considered TESS observations of KELT-9 b and found no evidence for decay. Continued monitoring, especially observations of planetary eclipses, seems likely to resolve whether the system actually experiences tidal decay, which would be especially surprising since A/B stars are not expected to exhibit significant tidal dissipation (Ogilvie 2014).

What to make of all these comparisons? One key conclusion is that statistical fluctuations in ΔBIC often appear and may falsely hint at tidal decay. Continued, sustained growth in ΔBIC is probably required to confidently report detection of tidal decay. A calculation like that depicted in the right panel of Figure 6 tailored for a specific campaign provides a way of assessing the threshold ΔBIC beyond which tidal decay may be plausible.

4. DISCUSSION AND CONCLUSIONS

The approach presented here allows observers to plan observational programs to maximize the possibility for detecting tidal decay while minimizing the required resources. This approach is framed in such a way that it does not, in principle, even require observations to make useful predictions: if observers have estimates for the expected transit timing uncertainty (Equation 11) and tidal decay rate (Equation 22), along with a planned observational sequence (which orbital epochs will be observed), Equation 34 provides a way of estimating the likelihood for detecting tidal decay.

Naturally, this approach comes with important caveats and limitations. For instance, we have assumed a linear regression approach, but real transit data may have complex and asymmetric uncertainties (Hagey et al. 2022) for which such an approach is only an approximation. Our approach also assumes the BIC provides an accurate means for comparing models with tidal decay and those without. However, the BIC is only valid for sample sizes much larger than the number of model parameters (Schwarz 1978). Fortunately, seeking signs of tidal decay necessitates a large number of observations, and so this requirement is likely always fulfilled in this context. Finally, we have limited our scope to tidal decay and have not explicitly considered other astrophysical processes that can affect the ephemeris. But our approach should apply to any mechanism that introduces a quadratic term into the ephemeris, so it should be able to capture the impact of precession on both transit and eclipse timings (Winn 2010). Our method can likely be extended to consider other simple ephemeris effects, as long as they can be readily captured by a linear regression approach.

Another potentially fruitful extension would be to incorporate a more sophisticated relationship between stellar properties and tidal decay rate. Studies of stellar tides suggest that the deeper convective zones in later-type (i.e., cooler) stars tend to promote tidal dissipation, resulting in smaller tidal dissipation parameters Q_* (e.g., Barker 2022), which would tend to recommend their planetary systems as good targets for detecting tidal decay. Main-sequence, cooler stars tend to be smaller, too, giving deeper transits and therefore smaller timing uncertainties (Equation 11). On the other hand, main-sequence cooler stars are dimmer, which tends to inflate the photometric uncertainty (Equation 12). Figuring out how to thread this needle and choose the best set of stars to optimize decay detection should be the subject of future work.

As discussed in Section 1, detecting tidal decay is critical for constraining Q_* and planetary engulfment rates. As pointed out in Metzger et al. (2012), the engulfment rate should scale roughly as Q_* , and if many stars had Q_* values as small as WASP-12’s, we might expect a galactic engulfment rate as large as 18 yr^{-1} . This value is likely overly large since there is reason to believe WASP-12 has unusually dissipative tides (Bailey & Goodman 2019). Determining the actual rate is important for future surveys for engulfment signatures since, the larger the rate, the fewer stars would need to be monitored to catch engulfment. By efficiently directing searches for tidal decay, the approach outlined here would feed forward to guide surveys to search for engulfment as well.

¹ We thank an anonymous referee for thoughtful feedback. This study was supported by a grant from NASA’s Exoplanet Research Program.

We start with an ephemeris that resembles Equation 20:

$$t(E) = T_0 + PE + \frac{1}{2} \left(\frac{dP}{dE} \right) E^2 + \Phi(E), \quad (1)$$

where $\Phi(E)$ represents the scatter associated with point E . We assume $\langle \Phi(E) \rangle \approx 0$. Applying standard linear regression (cf. Press et al. 2002), we have

$$\begin{aligned} T'_0 &= \frac{S_{E^2} S_t - S_E S_{Et}}{SS_{E^2} - S_E^2}, \\ P' &= \frac{SS_{Et} - S_E S_t}{SS_{E^2} - S_E^2} \end{aligned} \quad (2)$$

where

$$\begin{aligned} S_t &= \sum_{E \in \text{transits}} \left(t(E) / \sigma_{t(E)}^2 \right) \\ &\approx \frac{1}{2} \left(\frac{dP}{dE} \right) S_{E^2} + P S_E + T_0 S \\ S_{Et} &= \sum_{E \in \text{transits}} \left(t(E) E / \sigma_{t(E)}^2 \right) \\ &\approx \frac{1}{2} \left(\frac{dP}{dE} \right) S_{E^3} + P S_E + T_0 S_E. \end{aligned} \quad (3)$$

We can then incorporate these expressions into Equation 3 and separate out the terms involving dP/dE to arrive at Equation 32.

Software: `astropy` (Astropy Collaboration et al. 2013, 2018), `matplotlib` (Hunter 2007), `numpy` (Harris et al. 2020), `scipy` (Virtanen et al. 2020)

REFERENCES

- Aguilera-Gómez, C., Chanamé, J., Pinsonneault, M. H., & Carlberg, J. K. 2016, *ApJ*, 829, 127, doi: [10.3847/0004-637X/829/2/127](https://doi.org/10.3847/0004-637X/829/2/127)
- Astropy Collaboration, Robitaille, T. P., Tollerud, E. J., et al. 2013, *A&A*, 558, A33, doi: [10.1051/0004-6361/201322068](https://doi.org/10.1051/0004-6361/201322068)
- Astropy Collaboration, Price-Whelan, A. M., Sipőcz, B. M., et al. 2018, *AJ*, 156, 123, doi: [10.3847/1538-3881/aabc4f](https://doi.org/10.3847/1538-3881/aabc4f)
- Baştürk, Ö., Southworth, J., Yalçinkaya, S., et al. 2023, *MNRAS*, 521, 1200, doi: [10.1093/mnras/stad248](https://doi.org/10.1093/mnras/stad248)
- Bailey, A., & Goodman, J. 2019, *MNRAS*, 482, 1872, doi: [10.1093/mnras/sty2805](https://doi.org/10.1093/mnras/sty2805)
- Barker, A. J. 2022, *ApJL*, 927, L36, doi: [10.3847/2041-8213/ac5b63](https://doi.org/10.3847/2041-8213/ac5b63)
- Barros, S. C. C., Akinsanmi, B., Boué, G., et al. 2022, *A&A*, 657, A52, doi: [10.1051/0004-6361/202142196](https://doi.org/10.1051/0004-6361/202142196)
- Behrard, A., Sevilla, J., & Fuller, J. 2023, *MNRAS*, 518, 5465, doi: [10.1093/mnras/stac3435](https://doi.org/10.1093/mnras/stac3435)
- Bonomo, A. S., Desidera, S., Benatti, S., et al. 2017, *A&A*, 602, A107, doi: [10.1051/0004-6361/201629882](https://doi.org/10.1051/0004-6361/201629882)
- Carter, J. A., Yee, J. C., Eastman, J., Gaudi, B. S., & Winn, J. N. 2008, *ApJ*, 689, 499, doi: [10.1086/592321](https://doi.org/10.1086/592321)
- De, K., MacLeod, M., Karambelkar, V., et al. 2023, *Nature*, 617, 55, doi: [10.1038/s41586-023-05842-x](https://doi.org/10.1038/s41586-023-05842-x)
- Deeg, H. J., Ocaña, B., Kozhevnikov, V. P., et al. 2008, *A&A*, 480, 563, doi: [10.1051/0004-6361:20079000](https://doi.org/10.1051/0004-6361:20079000)
- Gu, P.-G., Lin, D. N. C., & Bodenheimer, P. H. 2003, *ApJ*, 588, 509, doi: [10.1086/373920](https://doi.org/10.1086/373920)
- Hagey, S. R., Edwards, B., & Boley, A. C. 2022, *AJ*, 164, 220, doi: [10.3847/1538-3881/ac959a](https://doi.org/10.3847/1538-3881/ac959a)
- Hamer, J. H., & Schlaufman, K. C. 2019, *AJ*, 158, 190, doi: [10.3847/1538-3881/ab3c56](https://doi.org/10.3847/1538-3881/ab3c56)
- Harre, J. V., Smith, A. M. S., Barros, S. C. C., et al. 2023, *A&A*, 669, A124, doi: [10.1051/0004-6361/202244529](https://doi.org/10.1051/0004-6361/202244529)
- Harris, C. R., Millman, K. J., van der Walt, S. J., et al. 2020, *Nature*, 585, 357, doi: [10.1038/s41586-020-2649-2](https://doi.org/10.1038/s41586-020-2649-2)
- Hunter, J. D. 2007, *Computing In Science & Engineering*, 9, 90
- Ivshina, E. S., & Winn, J. N. 2022, *ApJS*, 259, 62, doi: [10.3847/1538-4365/ac545b](https://doi.org/10.3847/1538-4365/ac545b)

- Jackson, B., Greenberg, R., & Barnes, R. 2008, *ApJ*, 678, 1396, doi: [10.1086/529187](https://doi.org/10.1086/529187)
- Jackson, B., Jensen, E., Peacock, S., Arras, P., & Penev, K. 2016, *Celestial Mechanics and Dynamical Astronomy*, 126, 227, doi: [10.1007/s10569-016-9704-1](https://doi.org/10.1007/s10569-016-9704-1)
- Jia, S., & Spruit, H. C. 2017, *MNRAS*, 465, 149, doi: [10.1093/mnras/stw1693](https://doi.org/10.1093/mnras/stw1693)
- MacLeod, M., Cantiello, M., & Soares-Furtado, M. 2018, *ApJL*, 853, L1, doi: [10.3847/2041-8213/aaa5fa](https://doi.org/10.3847/2041-8213/aaa5fa)
- Mannaday, V. K., Thakur, P., Southworth, J., et al. 2022, *AJ*, 164, 198, doi: [10.3847/1538-3881/ac91c2](https://doi.org/10.3847/1538-3881/ac91c2)
- Mayor, M., & Queloz, D. 1995, *Nature*, 378, 355, doi: [10.1038/378355a0](https://doi.org/10.1038/378355a0)
- Metzger, B. D., Giannios, D., & Spiegel, D. S. 2012, *MNRAS*, 425, 2778, doi: [10.1111/j.1365-2966.2012.21444.x](https://doi.org/10.1111/j.1365-2966.2012.21444.x)
- Ogilvie, G. I. 2014, *ARA&A*, 52, 171, doi: [10.1146/annurev-astro-081913-035941](https://doi.org/10.1146/annurev-astro-081913-035941)
- Patra, K. C., Winn, J. N., Holman, M. J., et al. 2017, *AJ*, 154, 4, doi: [10.3847/1538-3881/aa6d75](https://doi.org/10.3847/1538-3881/aa6d75)
- . 2020, *AJ*, 159, 150, doi: [10.3847/1538-3881/ab7374](https://doi.org/10.3847/1538-3881/ab7374)
- Press, W. H., Teukolsky, S. A., Vetterling, W. T., & Flannery, B. P. 2002, *Numerical recipes in C++ : the art of scientific computing*
- Qureshi, A., Naoz, S., & Shkolnik, E. L. 2018, *ApJ*, 864, 65, doi: [10.3847/1538-4357/aad562](https://doi.org/10.3847/1538-4357/aad562)
- Rappaport, S., Sanchis-Ojeda, R., Rogers, L. A., Levine, A., & Winn, J. N. 2013, *ApJL*, 773, L15, doi: [10.1088/2041-8205/773/1/L15](https://doi.org/10.1088/2041-8205/773/1/L15)
- Rasio, F. A., Tout, C. A., Lubow, S. H., & Livio, M. 1996, *ApJ*, 470, 1187, doi: [10.1086/177941](https://doi.org/10.1086/177941)
- Rosário, N. M., Barros, S. C. C., Demangeon, O. D. S., & Santos, N. C. 2022, *A&A*, 668, A114, doi: [10.1051/0004-6361/202244513](https://doi.org/10.1051/0004-6361/202244513)
- Schwarz, G. 1978, *Annals of Statistics*, 6, 461
- Valsecchi, F., Rappaport, S., Rasio, F. A., Marchant, P., & Rogers, L. A. 2015, *ApJ*, 813, 101, doi: [10.1088/0004-637X/813/2/101](https://doi.org/10.1088/0004-637X/813/2/101)
- Virtanen, P., Gommers, R., Oliphant, T. E., et al. 2020, *Nature Methods*, 17, 261, doi: [10.1038/s41592-019-0686-2](https://doi.org/10.1038/s41592-019-0686-2)
- Vissapragada, S., Chontos, A., Greklek-McKeon, M., et al. 2022, *ApJL*, 941, L31, doi: [10.3847/2041-8213/aca47e](https://doi.org/10.3847/2041-8213/aca47e)
- Weinberg, N. N., Sun, M., Arras, P., & Essick, R. 2017, *ApJL*, 849, L11, doi: [10.3847/2041-8213/aa9113](https://doi.org/10.3847/2041-8213/aa9113)
- Winn, J. N. 2010, in *Exoplanets*, ed. S. Seager, 55–77
- Wong, I., Shporer, A., Vissapragada, S., et al. 2022, *AJ*, 163, 175, doi: [10.3847/1538-3881/ac5680](https://doi.org/10.3847/1538-3881/ac5680)
- Yang, F., & Wei, X. 2022, *Publications of the Astronomical Society of the Pacific*, 134, 024401, doi: [10.1088/1538-3873/ac495a](https://doi.org/10.1088/1538-3873/ac495a)
- Yee, S. W., Winn, J. N., Knutson, H. A., et al. 2020, *ApJL*, 888, L5, doi: [10.3847/2041-8213/ab5c16](https://doi.org/10.3847/2041-8213/ab5c16)